Hydrothermal Synthesis of Anatase TiO$_2$ Nanoflowers on a Nanobelt Framework for Photocatalytic Applications

MEICHENG LI,[1,2,3,4] YONGJIAN JIANG,[2] RUIQING DING,[2] DANDAN SONG,[2] HANG YU,[2] and ZHAO CHEN[2]

1.—State Key Laboratory of Alternate Electrical Power System with Renewable Energy Sources, North China Electric Power University, Beijing 102206, China. 2.—School of Renewable Energy, North China Electric Power University, Beijing 102206, China. 3.—Su Zhou Institute, North China Electric Power University, Suzhou 215123, China. 4.—e-mail: mcli@ncepu.edu.cn

Anatase titanium dioxide (TiO$_2$) nanoflowers were fabricated on rutile TiO$_2$ nanobelts through a simple hydrothermal synthesis. The architecture of the composite nanostructures was composed of a rutile nanobelt framework with anatase nanoflowers. The novel TiO$_2$ composite nanostructures exhibit higher photocatalytic activity for organic pollutants relative to TiO$_2$ nanobelts and commercially available nanoparticles (P25). This enhanced photocatalytic activity is primarily a result of complex crystal nanostructures that enhance the carrier transport along the nanobelt framework. The results indicate that this novel TiO$_2$ nanostructure has superior photocatalytic properties, which demonstrates its potential as a new photocatalyst material.

Key words: TiO$_2$, nanoflower, hydrothermal synthesis, photocatalyst

INTRODUCTION

Titanium dioxide (TiO$_2$) is the most widely used photocatalyst due to its unique physical and chemical properties, environmental friendliness, and facile fabrication.[1–3] The application of TiO$_2$ is strongly dependent on its morphology, crystalline structure, and phase dimension.[4,5] The morphology and size properties of TiO$_2$ nanostructures determine their intrinsic properties, such as carrier transport and charge separation.[6–9] Hence, the characteristics of TiO$_2$ can be controlled by precise design of its nanostructure. Typically, a rough surface and good crystallization are essential for obtaining large specific surface areas with good carrier transport properties.[10] Structural control has been shown for nanoflower, nanoparticle, nanotube, and nanowire TiO$_2$, and these shapes along with rough surfaces and ordered structures have been shown to exhibit ideal behavior in photocatalytic applications.[11–13] The structures of TiO$_2$ that are commonly utilized tend to be on the nanoscale and show improvement with further decreases

in size; this makes reuse of these materials difficult and often results in other concerns regarding nanosized particles. To solve these problems, use of nanobelt architectures that are several tens of nanometers in width and have adjustable lengths has been examined.[10] Additionally, these nanobelts have characteristic high charge mobilities and fewer localized states near the band edges and in the bandgap due to the existence of fewer unpassivated surface states in the nanobelts, which reduces electron–hole recombination rates and therefore can enhance photocatalytic efficiencies.[13,14] While rutile nanobelts show good photocatalytic ability, they do not perform as well as other anatase nanostructures, such as nanoflower structures and nanosheet structures. One way to enhance the photocatalytic ability while maintaining the ability to reuse these materials may come from the development of new composite architectures.

In this study, we take advantage of the film layer petals composing anatase nanoflowers and the ability to isolate and reuse rutile nanobelts by proposing the growth of nanostructures on nanobelts and reporting on the resulting composite structures. A novel composite nanostructure is obtained by assembling flower-like nanostructures onto a TiO$_2$

nanobelt framework through a simple hydrothermal process. The resulting complex nanostructures exhibit good photocatalytic activity, showing its potential use as a photocatalyst.

EXPERIMENTAL PROCEDURES

Analytical-grade tetrabutyl titanate [Ti(OBu)$_4$] was used without further purification as the precursor for the growth of nanostructures on the surfaces of nanobelts. The experimental procedures were as follows. First, solutions of hydrochloric acid and deionized water were prepared. A certain volume of Ti(OBu)$_4$ was added dropwise into the aqueous HCl solutions, and the mixtures were stirred for 10 min until the solutions turned clear. Presensitized TiO$_2$ nanobelts that were prepared separately by the method provided in Ref. 10 were added to these solutions, which were then stirred for 30 min. The resulting solutions were transferred into 25-mL Teflon-lined stainless-steel autoclaves and sealed, followed by heat treatment at 423 K for preselected times. The resulting precipitates were washed with deionized water several times and dried at 333 K for 12 h under vacuum.

Photocatalytic degradation of organic dye MO was conducted under a 20 W power, 365 nm wavelength ultraviolet (UV) lamp at room temperature. Then, the prepared 100 mg/L TiO$_2$ composite architectures powder and 20 mg/L MO dye solution were placed into a 100-mL beaker. The mixed solution was firstly stirred in the dark until it became uniform, then exposed to UV light irradiation. Each sample's supernatant liquid was extracted every 15 min for further MO content testing. The decrease in the concentration of dye solution was measured with a spectrophotometer at max = 465 nm at specific reaction intervals. The adsorption experiments were carried out to investigate the adsorption of MO on the TiO$_2$ composite architectures. The above-mentioned mixed solution was (still in the dark) stirred for 60 min to obtain a good dispersion and establish adsorption–desorption equilibrium between the organic molecules and the catalyst surface. Thereafter, the sample's supernatant liquid was extracted to assess the concentration of MO remaining in the solution. For comparison, we repeated this experiment with P25 under the same experimental conditions. The UV source was a Cure Spot 50 (ADAC systems) equipped with an Hg lamp; the wavelength range was from 300 nm to 800 nm, and the light intensity was 2 mW/cm^2.

Electron scanning microscopy (SEM) measurements were obtained using a FEI Quanta200F microscope. X-ray powder diffraction (XRD) patterns of samples were examined by a Bruker D8 Focus x-ray powder diffractometer with Cu K$_\alpha$ radiation ($\lambda = 1.5406$ Å). The photocatalytic experiments were carried out using a UV–Vis spectrophotometer (Shimadzu UV2450).

RESULTS AND DISCUSSION

TiO$_2$ composite nanostructures were fabricated through a hydrothermal process as outlined in the "Experimental Procedures" section. Figure 1 shows SEM images of prepared nanobelts and the resulting nanostructures with rutile nanobelt branches and anatase nanoflowers covering the surfaces. The nanobelts are shown in Fig. 1a and b, A, and the nanoflowers are shown in Fig. 1b, B. The surfaces of the TiO$_2$ nanoflowers are composed of a spiral stamen and thin-layered petals. It can be seen from Fig. 1b that the TiO$_2$ nanoflowers are neatly arranged on the nanobelts, forming a flower–ribbon structure with average length of 1.5 μm to 2 μm. Meanwhile, the experiment showed that the nanobelt was treated as a framework for the formation of nanoflowers; when the amounts of added nanobelt and Ti(OBu)$_4$ were 0.02 g and 1.5 mL, 0.228 g of final product was obtained. The final product results from the additional precipitation of Ti(OBu)$_4$ precursor onto the TiO$_2$ nanobelts, corresponding to the weight change of the TiO$_2$ nanobelts after the reaction.

To clarify the formation mechanism of the flower nanostructures, we analyzed the factors affecting the nanostructure formation. The addition of the nanobelts played a crucial role in the formation of the composite nanostructures. To determine the effect of the addition of TiO$_2$ nanobelts, we varied the dose of TiO$_2$ nanobelts added to the reactant solutions, and the resulting TiO$_2$ nanostructures are shown in Fig. 2. The morphologies resulting from growth with Ti(OBu)$_4$ and HCl reactants without including nanobelts exhibit sphere-like structures with variable diameters from tens of nanometers to several micrometers, as shown in Fig. 2a. When 0.02 g of TiO$_2$ nanobelts was added to the reactants, the resulting morphology showed quite a different structure, with a complex strip surface covered by many flower-like nanostructures, as shown in Fig. 2b. When the amount of TiO$_2$ nanobelts was further increased to 0.1 g, a composite nanostructure was still obtained, but a large number of nanobelts were also observed independent of the flower structures, as shown in Fig. 2c.

To verify that the nanoflowers are formed on the surface of the nanobelts, we studied the addition of different concentrations of Ti(OBu)$_4$. The results are shown in Fig. 3. We found that the composition of the TiO$_2$ nanostructures exhibited a gradual evolution with increasing concentration of Ti(OBu)$_4$, indicating that the nanoflowers were formed at the surface of the complex nanostructures and were derived from the Ti(OBu)$_4$ through hydrolysis to TiO$_2$, followed by their organized growth on the TiO$_2$ nanobelts. When Ti(OBu)$_4$ was added to the solution, TiO$_2$ nanoflowers began to grow on nanobelts as shown in Fig. 3a, b. Increased addition of Ti(OBu)$_4$ led to an increase in the number of TiO$_2$ nanoflowers grown on nanobelts, as shown in
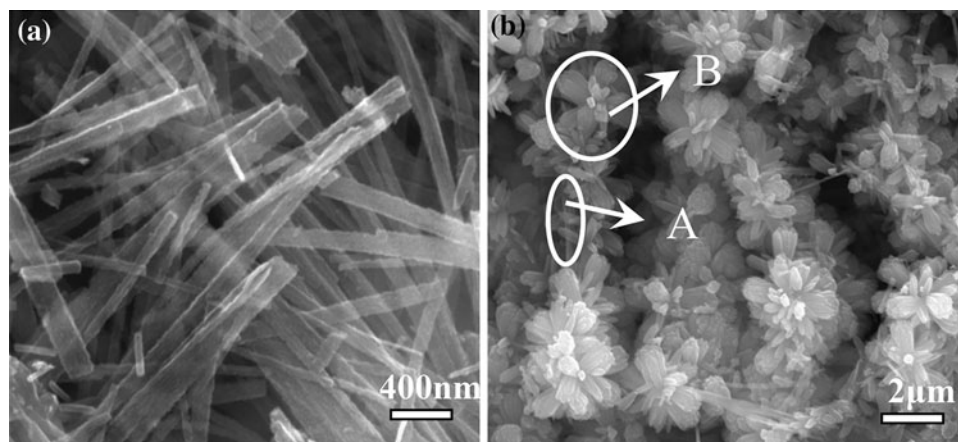
Fig. 1. SEM images of (a) TiO_2 nanobelts, (b) composite nanostructures composed of a rutile nanobelt framework with anatase nanoflowers: (A) nanobelt as framework, (B) nanoflower grown on nanobelt.
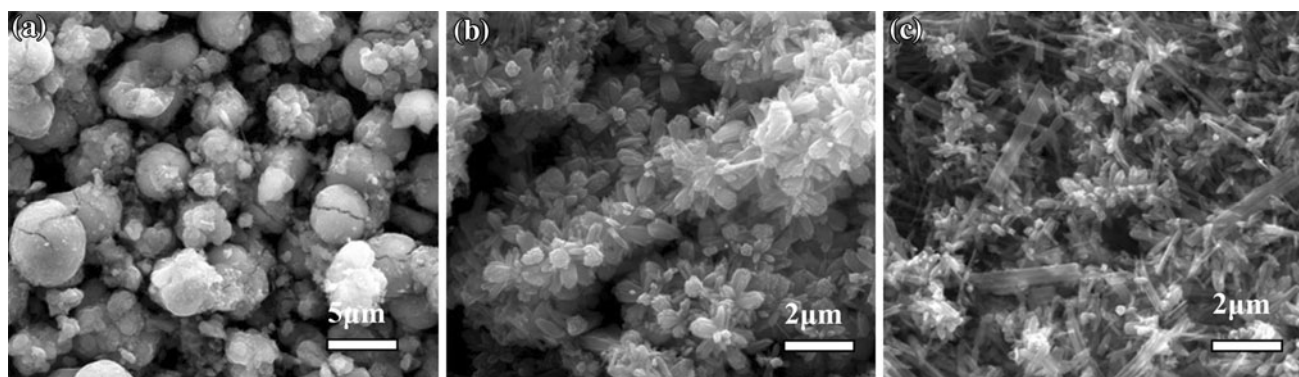

Fig. 2. SEM images of nanostructures obtained using different amounts of TiO_2 nanobelts: (a) 0 g, (b) 0.02 g, and (c) 0.1 g.

Fig. 3c. However, when too much $Ti(OBu)_4$ was added, the product appeared to agglomerate, as shown in Fig. 3d.

The time evolution of these composite nanostructures was also studied. From further analysis, it was found that, with increasing reaction time, the hydrolysis of $Ti(OBu)_4$ gradually increased, and the TiO_2 particles generated assembled into ordered nanostructures as shown in Fig. 4a–d. When the reaction time exceeded 12 h, the TiO_2 nanobelts were completely covered by nanoflowers as shown in Fig. 4d.

It is well known that the growth process of Ti^{4+} nanostructures is affected by both the amount and the hydrolysis rate of $Ti(OBu)_4$,[11] and thus to study the organization process of Ti^{4+}, we adjusted the hydrolysis rate of $Ti(OBu)_4$ by varying the volume ratio of HCl and H_2O. The hydrolysis rate of $Ti(OBu)_4$ was gradually reduced with increasing HCl concentration. We found that the preferential growth of TiO_2 molecules on the surface of the nanobelts led to the formation of ordered complex nanostructures where the nanoflowers became neatly arranged on a nanobelt support framework.

Based on these results, we propose a formation process for these TiO_2 composite nanostructures, as shown in Fig. 5. Different reaction times lead to different levels of hydrolysis of the $Ti(OBu)_4$, and therefore different amounts of TiO_2 crystal nuclei exist in the solution. With shorter reaction time (2 h), the $Ti(OBu)_4$ hydrolysis process begins, and crystal nuclei form randomly on the surface of the TiO_2 nanobelts. Because this reaction is time limited, most of the $Ti(OBu)_4$ did not have sufficient time to hydrolyze, and this is the stage where the formation of the flower-like nanostructures is initiated. During this stage, the crystal nuclei form in sprout-like structures, and as time increases, the hydrolysis of $Ti(OBu)_4$ increases, and a large number of TiO_2 crystal nuclei aggregate and tend to form sheet-like nanostructures. At this stage, the flower-like nanostructure is not obvious, but the direction of growth along the nanobelts can be clearly observed, and this is where the formation of multiple nanosheets around a center point begins. The flower-like nanostructures can be clearly observed at 8 h, owing to the variation in TiO_2 growth rates on different crystal planes.[11] If the extent of reaction is sufficient for growth, the TiO_2 nanobelt becomes surrounded by the flower-like TiO_2 structures, resulting in the formation of "flower–belts." With increasing HCl concentration, the hydrolysis rate of $Ti(OBu)_4$ is
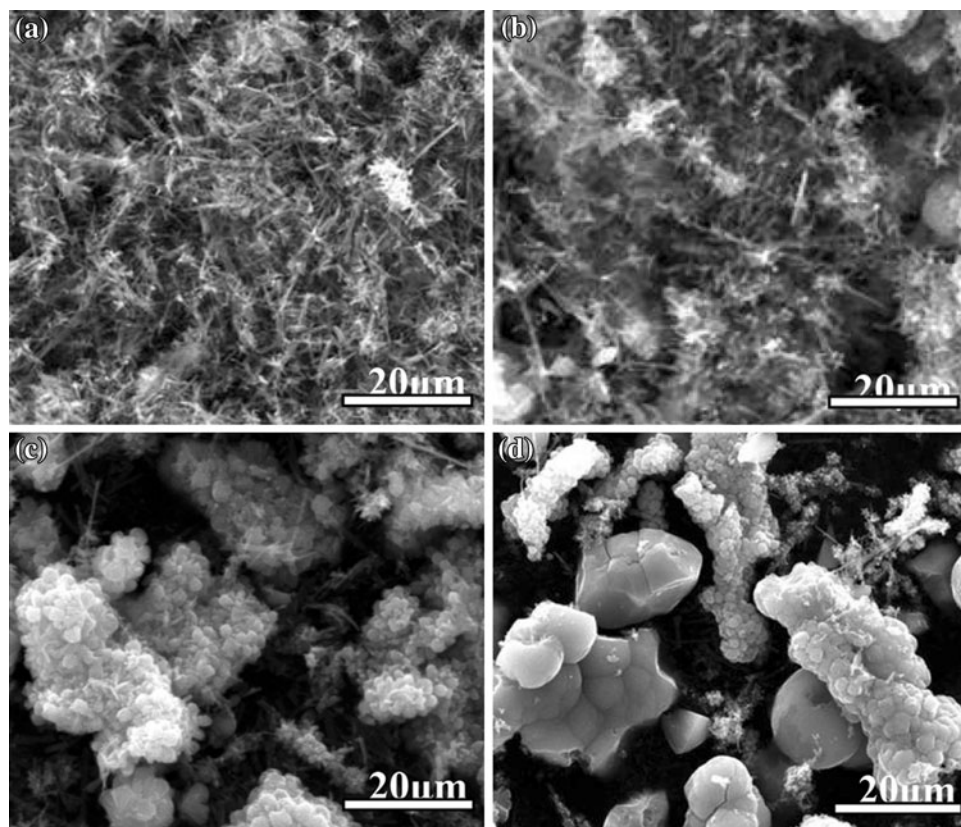
Fig. 3. SEM images of TiO_2 nanostructures obtained using different doses of $Ti(OBu)_4$: (a) 0.5 mL, (b) 1.0 mL, (c) 1.5 mL, and (d) 2.0 mL.

gradually reduced; we also found that Cl^- may be adsorbed by the surface of the TiO_2 nanobelts and blocked further hydrolysis of $Ti(OBu)_4$. The resulting TiO_2 molecules deposited on the surface of the nanobelts and grew in preferential directions on the nanobelt surfaces, resulting in the formation of flower-like nanostructures at the surface of the nanobelt, as shown in Fig. 6. We also found that, where the nanobelts overlap, more TiO_2 from the hydrolysis of $Ti(OBu)_4$ was deposited, representing locations where flower buds were easily formed, as seen in Fig. 6a, b. According to the theory of nucleation and growth, at the center of the overlap of the nanobelts, spiral growth can occur where the flower buds can form after the primary nucleation process,[15] and this represents the fringe of the nucleation center where the flower petals form according to the layer growth theory.[16]

To determine the crystal phase of the complex nanostructures, powder x-ray diffraction (XRD) patterns of the samples were recorded. Figure 7 shows an x-ray diffraction (XRD) pattern of the TiO_2 composite nanostructures, where the characteristic diffraction peaks of the TiO_2 composite nanostructures can be observed. A comparison with the diffraction peaks from pure rutile TiO_2 and pure anatase TiO_2 shows that both anatase (nanoflower) and rutile TiO_2 (nanobelt) phases exist in the TiO_2 complex nanostructures. The shapes of the diffraction

peaks suggest that the products are highly crystalline. We know that rutile TiO_2 nanobelts are obtained from heat treatment,[17] and the intensity and width of the strong (110) peak indicate that there is preferred anisotropic growth along the (110) crystal planes for the rutile TiO_2 nanobelts. By means of a low-temperature treatment, anatase TiO_2 nanoflowers are formed from the hydrolysis of tetrabutyl titanate, and the anatase TiO_2 nanoflower growth can be related to the surface electrostatic charge.[18] The anatase TiO_2 (101) peak indicates that the flower nanostructures are dominant on the {101} facets. We can also observe from the XRD pattern that there are peak interactions between the anatase and rutile TiO_2.

The refractive index of rutile TiO_2 is higher than that of anatase TiO_2, and addition of a small amount of rutile TiO_2 will benefit anatase TiO_2 by enhancing several parameters, including the absorption of light, the photon capture rate, the battery current, and the transmission of light. Anatase TiO_2 has a higher photoelectric conversion efficiency because the electronic transfer rate of anatase TiO_2 is higher than that of rutile TiO_2. A mixture of the two polymorphs yields an even higher photocatalytic activity for specific ratios. This enhancement is attributed to the specific electronic states of the two crystal structures, which allow for a semiconductor–semiconductor junction.[19]
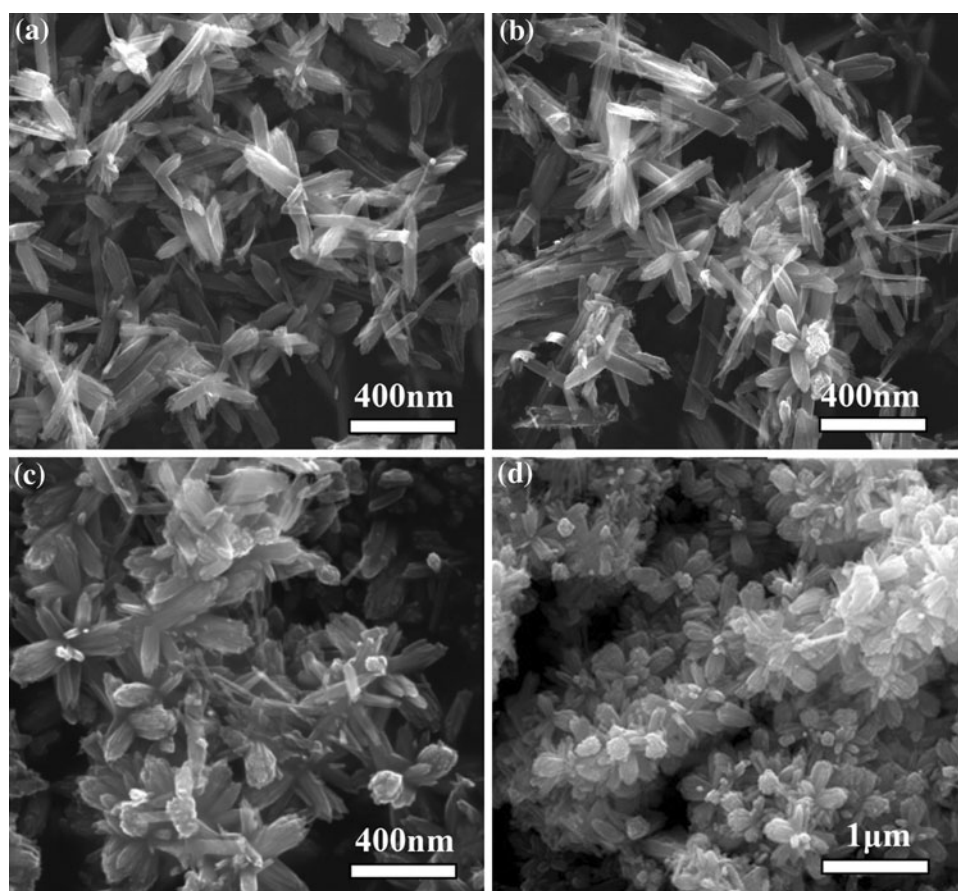
Fig. 4. SEM images of TiO$_2$ nanostructures obtained after different reaction times: (a) 2 h, (b) 5 h, (c) 8 h, and (d) 12 h.
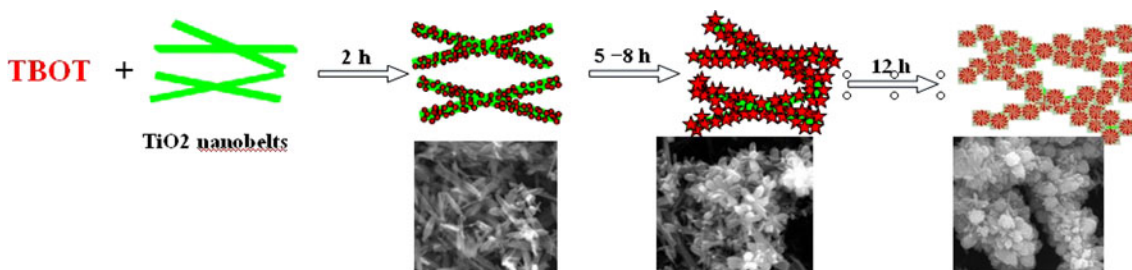

Fig. 5. Schematic illustration of the formation process for the TiO$_2$ flower-like nanostructures for different reaction times. Green represents the TiO$_2$ nanobelts; Red represents the TiO$_2$ formed from the hydrolysis of Ti(OBu)$_4$ (color figure online).

Hence, the composite nanostructures obtained in this work by use of the anatase and rutile polymorphs have the potential to exhibit higher photocatalytic activity.

The photocatalytic activities of the prepared TiO$_2$ composite nanostructures, neat TiO$_2$ nanobelts, and commercially available P25[20] were evaluated for the degradation of MO. After irradiation under UV light at room temperature for 60 min, the absorbance of the dye solution of these three samples was measured, the results of which are shown in Fig. 8. It can be seen that the TiO$_2$ composite nanostructure exhibits the highest photocatalytic activity. This is

due to its special nanostructure and the presence of both anatase and rutile TiO$_2$. The nanobelts play an important role in closely connecting the flower-like TiO$_2$, while at the same time serving to increase the speed of electronic transfer, thus improving the photocatalytic properties of the complex nanostructure.

Some systematic research was carried out to study the process of MO degradation. Firstly, as shown in Fig. 9, the adsorption of MO by P25 and TiO$_2$ composite nanostructures was measured. The P25 has larger specific surface area (73 m^2/g) compared with the TiO$_2$ composite nanostructures
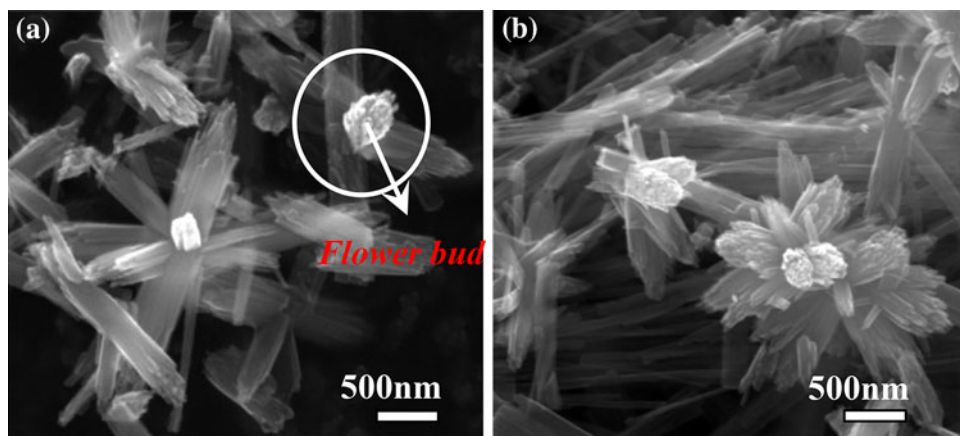
Fig. 6. SEM images of growth details of TiO$_2$ nanoflowers on TiO$_2$ nanobelts: (a) the flower bud began to grow at the location of nanobelt overlap; (b) nanoflower grown on the nanobelt.
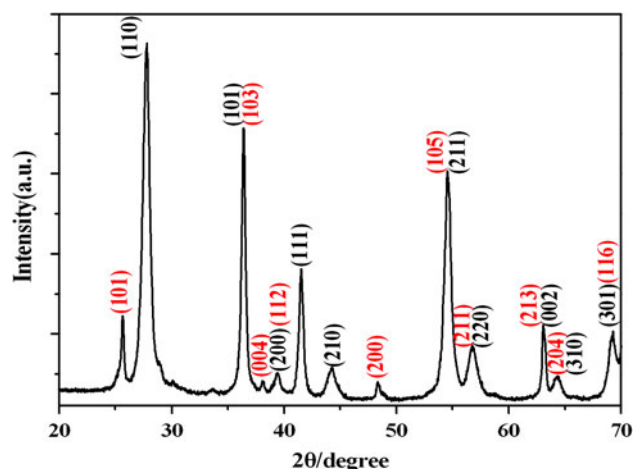

Fig. 7. XRD pattern of the TiO$_2$ complex nanostructures; red labels correspond to anatase form, whereas black labels correspond to rutile forms (color figure online).
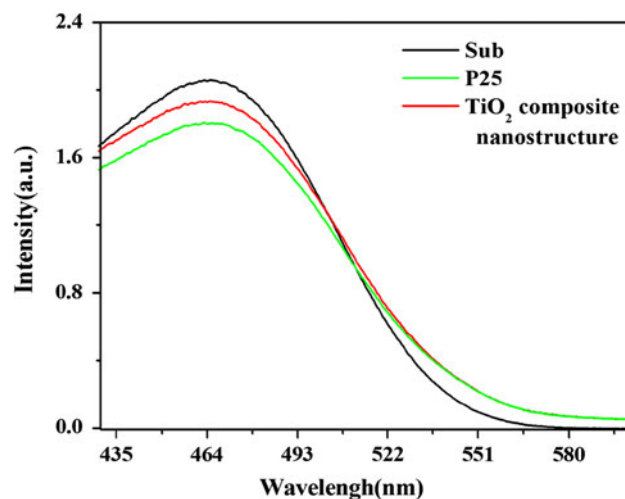

Fig. 9. Adsorption of MO by P25 and TiO$_2$ composite nanostructures after stirring in the dark for 60 min at room temperature (color figure online).
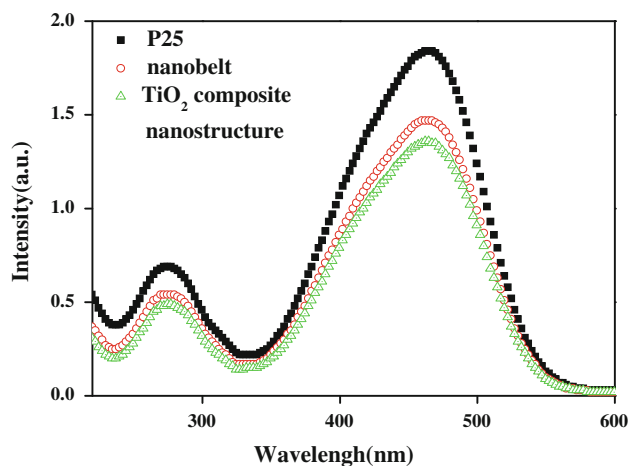

Fig. 8. UV–Vis absorption spectra of TiO$_2$ composite nanostructure, TiO$_2$ nanobelts, and commercially available P25 at room temperature (color figure online).
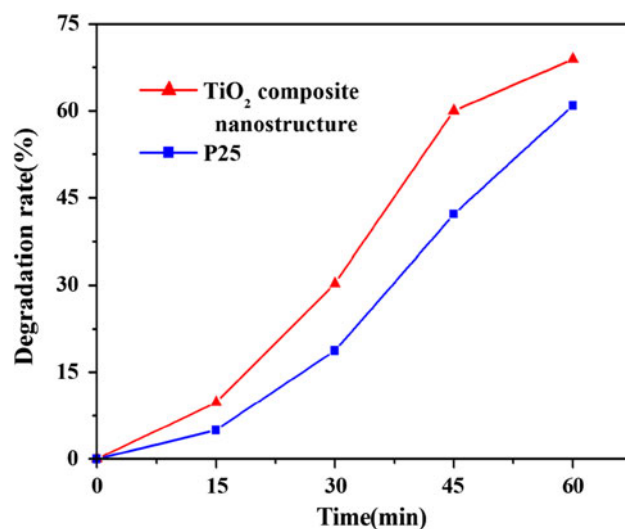

Fig. 10. Degradation rates after different times for P25 and TiO$_2$ composite nanostructures (color figure online).

(21 m^2/g), since the P25 exhibits better ability in terms of MO adsorption. Secondly, the MO degradation rates by P25 and TiO$_2$ composite nanostructures at different times were measured by spectrophotometer at 465 nm. As shown in Fig. 10, the TiO$_2$ composite nanostructures showed better degradation rates compared with P25 during 60 min. After illumination under UV light for 60 min, the degradation rate of the TiO$_2$ composite nanostructures increased to 68%, being 10% higher than that of P25. These results indicate that the novel composite nanostructures obtained in this work may act as potential photocatalyst candidates.

CONCLUSIONS

A novel approach for the formation of composite TiO$_2$ nanostructures is proposed by realizing the assembly of anatase TiO$_2$ nanoflowers on rutile TiO$_2$ nanobelts through a simple hydrothermal synthesis, and the formation mechanism is studied in detail. The TiO$_2$ complex nanostructure possesses good crystallinity with the presence of both anatase TiO$_2$ nanoflowers and rutile TiO$_2$ nanobelts, and the existence of this double-crystal phase shows high photocatalytic activities for organic pollutants. The improvement in photocatalysis over neat anatase and rutile forms of TiO$_2$ supports this material's potential in environmental purification, water photoelectrolysis, and solar energy utilization.

ACKNOWLEDGEMENTS

REFERENCES

1. X. Chen and S.S. Mao, *Chem. Rev.* 107, 2891 (2007).
2. B. O'Regan and M. Gratzel, *Nature* 353, 737 (1991).
3. Z.R. Tian, J.A. Voigt, J. Liu, B. McKenzie, and H. Xu, *J. Am. Chem. Soc.* 125, 12384 (2003).
4. C. Burda, X. Chen, R. Narayanan, and M.A. El-Sayed, *Chem. Rev.* 105, 1025 (2005).
5. X.F. Yang, C.J. Jin, C.L. Liang, D.H. Chen, M.M. Wu, and Y.C. Jimmy, *Chem. Commun.* 47, 1184 (2011).
6. K.S. Brammer, S.H. Oh, J.O. Gallagher, and S.H. Jin, *Nano Lett.* 8, 786 (2008).
7. M. Casavola, V. Grillo, E. Carlino, C. Giannini, F. Gozzo, E.F. Pinel, M.A. Garcia, L. Manna, R. Cingolani, and P.D. Cozzoli, *Nano Lett.* 7, 1386 (2007).
8. R. Buonsanti, V. Grillo, E. Carlino, C. Giannini, T. Kipp, R. Cingolani, and P.D. Cozzoli, *J. Am. Chem. Soc.* 130, 11223 (2008).
9. M.Z. Tang and J.M. Wu, *Sci. Adv. Mater.* 1, 144 (2009).
10. Y.M. Wang, G.J. Du, H. Liu, D. Liu, S.B. Qin, N. Wang, C.G. Hu, X.T. Tao, J. Jiao, J.Y. Wang, and Z.L. Wang, *Adv. Funct. Mater.* 18, 1131 (2008).
11. W.J. Zhou, X.Y. Liu, J.J. Cui, L. Duo, J. Li, H.D. Jiang, J.Y. Wang, and H. Liu, *Cryst. Eng. Comm.* 13, 4557 (2011).
12. C. Luis and T. Mauricio, *Phys. B* 390, 143 (2007).
13. Y.Y. Li, J.P. Liu, and Z.J. Jia, *Mater. Lett.* 60, 1753 (2006).
14. Wu M, Li Y, Deng Z (2011) Chem Sus Chem. Wiley Online Library.
15. P. Smereka, *Phys. D* 138, 282 (2000).
16. J. Aarik, A. Aidla, V. Sammelselg, and T. Uustare, *Thin Solid Films* 370, 163 (2000).
17. J.N. Nian and H. Teng, *J. Phys. Chem. B* 110, 4193 (2006).
18. K. Woan, G. Pyrgiotakis, and W. Sigmund, *Adv. Mater.* 21, 2233 (2009).
19. X. Zhang, A. Gu, G. Wang, B. Fang, Q. Yan, J. Zhu, T. Sun, J. Ma, and H.H. Hng, *Cryst. Eng. Comm.* 13, 188 (2011).
20. R. Ma, T. Sasaki, and Y. Bando, *J. Am. Chem. Soc.* 126, 10382 (2004).